Effective DQE (eDQE) and speed of digital radiographic systems: An experimental methodology

Ehsan Samei[a)]
Departments of Radiology, Biomedical Engineering, and Physics, Carl E. Ravin Advanced Imaging Laboratories (RAI Labs), Medical Physics Graduate Program, Duke University and Medical Center, 2424 Erwin Road, Suite 302, Durham, North Carolina 27705

Nicole T. Ranger
Department of Radiology, Carl E. Ravin Advanced Imaging Laboratories (RAI Labs), Duke University and Medical Center, 2424 Erwin Road, Suite 302, Durham, North Carolina 27705

Alistair MacKenzie
Department of Medical Engineering and Physics, KCARE, Faraday Building, King's College Hospital, Denmark Hill, London SE5 9RS, United Kingdom

Ian D. Honey
Department of Medical Physics Floor 3, Henriette Raphael House, Guy's and St Thomas Hospital, London SE19RT, United Kingdom

James T. Dobbins III
Departments of Radiology and Biomedical Engineering, Carl E. Ravin Advanced Imaging Laboratories (RAI Labs), Medical Physics Graduate Program, Duke University and Medical Center, 2424 Erwin Road, Suite 302, Durham, North Carolina 27705

Carl E. Ravin
Department of Radiology, Carl E. Ravin Advanced Imaging Laboratories (RAI Labs), Duke University and Medical Center, 2424 Erwin Road, Suite 302, Durham, North Carolina 27705

(Received 11 July 2008; revised 11 June 2009; accepted for publication 12 June 2009; published 23 July 2009)

Prior studies on performance evaluation of digital radiographic systems have primarily focused on the assessment of the detector performance alone. However, the clinical performance of such systems is also substantially impacted by magnification, focal spot blur, the presence of scattered radiation, and the presence of an antiscatter grid. The purpose of this study is to evaluate an experimental methodology to assess the performance of a digital radiographic system, including those attributes, and to propose a new metric, *effective* detective quantum efficiency (eDQE), a candidate for defining the efficiency or *speed* of digital radiographic imaging systems. The study employed a geometric phantom simulating the attenuation and scatter properties of the adult human thorax and a representative indirect flat-panel-based clinical digital radiographic imaging system. The noise power spectrum (NPS) was derived from images of the phantom acquired at three exposure levels spanning the operating range of the clinical system. The modulation transfer function (MTF) was measured using an edge device positioned at the surface of the phantom, facing the x-ray source. Scatter measurements were made using a beam stop technique. The eDQE was then computed from these measurements, along with measures of phantom attenuation and x-ray flux. The MTF results showed notable impact from the focal spot blur, while the NPS depicted a large component of structured noise resulting from use of an antiscatter grid. The eDQE was found to be an order of magnitude lower than the conventional DQE. At 120 kVp, eDQE(0) was in the 8%–9% range, fivefold lower than DQE(0) at the same technique. The eDQE method yielded reproducible estimates of the system performance in a clinically relevant context by quantifying the inherent speed of the system, that is, the actual signal to noise ratio that would be measured under clinical operating conditions.
[DOI: 10.1118/1.3171690]

Key words: image quality, modulation transfer function (MTF), noise power spectrum (NPS), detective quantum efficiency (DQE), chest radiography, digital radiography, speed

I. INTRODUCTION

In analog screen-film systems, the concept of speed has been well established as the exposure or air KERMA needed to achieve a certain level of optical density (i.e., analog signal) on the film and is inversely related to exposure.[1] The use of optical density as the basis for speed is well justified in analog systems employing film since, with all other factors held constant, for a given imaging geometry and technique, the contrast resolution (as predicted by optical density) is a key attribute of image quality. In digital systems, however, the

acquisition and display functions of the image formation are separated; consequently, the quality of the image is no longer governed by signal strength alone but by the image signal-to-noise ratio (SNR). With this shift from contrast-limited to SNR-limited imaging, one may argue that the proper use of a digital system in terms of the required dose or exposure should no longer be based on the x-ray flux required to achieve a certain signal strength but that needed to obtain a desired level of SNR in the final image.

Characterizing the SNR performance of an imaging detector in the context of how efficiently it utilizes the limited number of incident x-ray photons during the process of image formation, the detective quantum efficiency (DQE) has become a common metric of image quality for digital radiography and mammography systems.[2–10] However, while objective and quantitative, the DQE does not reflect the contributions of scattered radiation, antiscatter grid, magnification, and focal spot (FS) blur on the quality of images acquired clinically.[11,12] In the past five years, both our laboratory and another research group independently developed methodologies to include these effects into an overall system DQE. Kyprianou and co-workers[13–18] developed a formalism called "generalized DQE (GDQE)" and our group developed a concept called "effective DQE (eDQE)." These two approaches are similar in many respects but differ in a few details. The GDQE of Kyprianou and co-workers includes the frequency spectrum of the scattered radiation, whereas our eDQE includes the net effect of scatter on modulation transfer function (MTF) but ignores the frequency response of scatter below 0.1 mm^{-1}, except for the zero frequency drop. Both techniques include the effect of magnification, and Kyprianou and co-workers included focal spot blur; our eDQE approach originally did not include the effects of focal spot blur but that has recently been included. The GDQE method of Kyprianou and co-workers defines a system DQE at arbitrary depth, but our eDQE is primarily defined at a given distance from the detector with a specified phantom. Although both GDQE and eDQE are applicable to a variety of imaging devices, evaluations of GDQE in literature have largely focused on microangiographic applications and eDQE has focused on chest and mammographic applications. Despite these differences, the objectives of GDQE and eDQE are similar. This paper extends our work to include experimental measurement on chest radiography systems and also the concept of using eDQE as a measure of system speed.

The purpose of this study was to develop an experimental methodology to quantitatively assess the performance of a clinical digital radiographic system in the presence of scattered radiation, antiscatter grid, magnification, and focal spot blur. The methodology involves the measurement of the DQE in the presence of these additional system attributes to determine an *effective* detective quantum efficiency (eDQE) which would be applicable to the overall image acquisition *system*, as opposed to the detector only. The concept is not directly applicable to the entire imaging system (including processing and display components) rather the acquisition component only. An important application of the concept of the eDQE is its utility to serve as an application-specific definition of speed for digital radiographic and mammographic systems such that a target incident exposure (or dose) may be determined based on the desired SNR response from the imaging system.

II. MATERIALS AND METHODS

II.A. Phantom

The study was based on a phantom designed by the Food and Drug Administration (FDA) for use in the nationwide evaluation of x-ray trend (NEXT) program.[19,20] The phantom consisted of 25.4×25.4 cm^2 slabs of acrylic and aluminum, separated by an air gap, to emulate the attenuation and scatter conditions representative of adult chest radiography (Fig. 1). It also included a stand for the placement of an ionization chamber in the beam to provide consistent measurement of in-air exposure during an image acquisition.

II.B. Imaging system

A typical digital radiographic imaging system was used as a platform for the development of the measurement methodology. The system (Revolution XQ/i, GE Healthcare, Milwaukee, WI) employed a 0.2-mm-pitch indirect flat-panel detector, a source to image distance (SID) of 180 cm, and a stationary grid with 78 lines/cm, 20 μm Pb strips with Al interspace, and a grid ratio of 13:1 (Mitaya Manufacturing Co Ltd, Tokyo, Japan), as used in routine clinical chest exams with the system. A second identical system installed at another institution was also employed to assess the reproducibility of the results and system performance. Both systems were tested under operating conditions representative of those used clinically. These conditions included the applicable calibrations, choice of grid, two operating kVps (90 and 120), and two sizes for the focal spot (0.6 and 1.25 mm). Prior to the evaluation each system was calibrated without the grid in place per the manufacturer's protocol as is typical for digital radiography systems with a removable grid. All image data were obtained from the systems in the "for-processing" format, with postacquisition processing steps of the data only limited to gain, offset, and bad-pixel calibrations.

The system response function was measured following an established methodology,[2] but with the phantom placed in proximity to the x-ray source to simulate the effects of the primary beam filtration/hardening.[5] Exposures were measured free-in-air using a calibrated ionization chamber (MDH models 1015 and 2025, 10X5-6 ionization chamber, Radcal, Monrovia, CA). All exposure values were then inverse-square corrected to reflect the exposure at the detector plane. Both systems demonstrated excellent linearity between pixel value and exposure. As the two systems were found to have similar response characteristics at both kVps (i.e., linear behavior with zero intercepts, the main prerequisites for our data analysis). Based on the measured system response function, as denoted in Table I, all image pixel val-

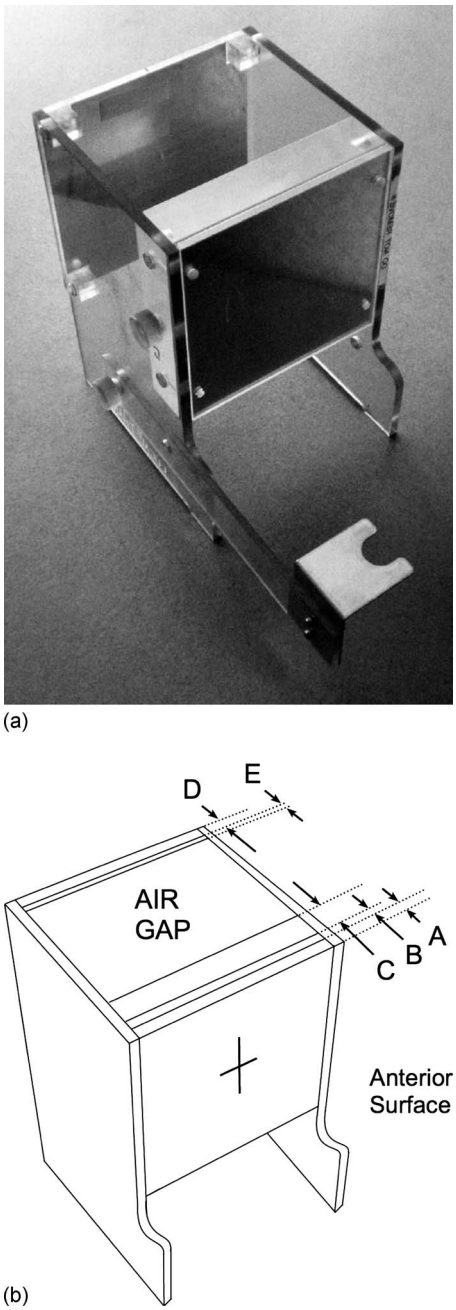

FIG. 1. The FDA chest phantom deployed for this study (a) showing its geometry and composition in side view (b); A=9.5 mm acrylic, B=2.5 mm Al, C=54.0 mm acrylic, D=9.5 mm acrylic, E=1.6 mm Al, and air gap between C and E layers=190.0 mm.

ues (Q) were transformed to have a generalized relationship with exposure (E) as $Q=4000E$, enabling a constant representation of image data across all images.

II.C. Transmission and scatter measurements

The narrow beam transmission fraction (TF) through the phantom was measured at 90 and 120 kVp as the ratio of the average exposure (across five repeats) with the phantom present to that without. Exposure measurements were made using a calibrated ionization chamber (MDH models 1015 and 2025, 10X5-6 ionization chamber, Radcal, Monrovia, CA), with the phantom and probe positioned along the beam axis at approximately one-third and two-thirds, respectively, of the SID (180 cm) from the x-ray source, and with the x-ray beam collimated to the approximate size of the ionization probe with a margin for error to ensure the flux on the ionization probe was uniform. For reference, the transmission fraction through the phantom was also measured using a wide-beam geometry with a beam size reflective of that used clinically on the system, i.e., the beam covering the full detector, and with the ionization chamber positioned at a distance of 5 cm from the beam exit surface of the phantom to reflect the approximate distance between the detector plane and the detector outer cover. For this measurement, the ionization chamber and phantom were positioned along the beam axis at more than 30 cm away from the detector to avoid backscattered radiation that might otherwise be captured by the chamber.

The scatter response of the system was evaluated with the phantom using a beam stop technique.[21,22] A beam stop array device was placed adjacent to the surface of the phantom facing the x-ray source, with the phantom centered in the field of view and adjacent to the detector cover plate (Fig. 2). The beam stop array device was composed of a 14×16 array of 224 Pb cylinders spaced 25 mm apart, each 6 mm in thickness and 3 mm in diameter, embedded in a 6-mm-thick sheet of polystyrene. Three images of the device were captured at 90 and 120 kVp at a relatively high exposure setting, $3.2E_0$, where E_0 is the free-in-air exposure level (inverse-squared corrected to the exposure at the detector) that would approximately deliver the desired target exposure (E_{nl} using the IEC terminology) to the detector (i.e., 0.4 mR) in the presence of phantom and grid as specified by the system manufacturer. Mean pixel values were measured within a 10 pixel$\times$10 pixel region of interest (ROI) positioned over each beam stop and ROIs on either side of the beam stop. The scatter fraction was then computed from the ratio of attenuated to average background counts averaged across 20 beam stops in the central portion of the image (Fig. 3).

II.D. Noise measurements

The noise performance of the systems was measured with the phantom placed at the detector cover plate (Fig. 2). Images of the phantom were obtained at 90 and 120 kVp at three exposure levels corresponding to $E_0/3.2$, E_0, and $3.2E_0$, where E_0 is the free-in-air exposure level (inverse-square corrected to the plane of the detector) that would approximately deliver the desired target exposure to the detector (i.e., 0.4 mR) in the presence of phantom and grid as specified by the system manufacturer. At each exposure condition, ten repeat images were acquired to exceed a total of 4 000 000 (IEC-specified) independent pixels in a central 18×18 cm^2 area within the phantom region of the image.[5] The image data were then processed to compute the noise power spectrum (NPS) using an established technique.[3,23] The processing steps included the division of the central 18×18 cm^{-2} area of each image into a total of 49 sequential

TABLE I. Basic characteristics of imaging systems tested in the study. XQ/i-1 and XQ/i-2 refer to two systems of the same make and model installed and tested at two different institutions. The approximate exposure received by the detector (the last column) is obtained by multiplying the reported exposure values by the wide-angle phantom transmission fraction (17.5% and 13.6% at 120 and 90 kVp, respectively) and the grid transmission fraction (approximately 48%).

System	Beam quality (kV)	Nominal focal spot size (mm)	q-value ($mR^{-1}\,mm^{-2}$)	Relationship of pixel value (Q) and exposure (E in mR)	Scatter fraction (%)	Phantom transmission fractions	Incident exposures (mR) $\sim E_0/3.2$ $\sim E_0$ $\sim 3.2E_0$	Detector exposures (mR) $\sim E_{nl}/3.2$ $\sim E_{nl}$ $\sim 3.2E_{nl}$
GE XQ/i-1	120	1.25	255 100	Q=1132.2E+33.8 (R^2=0.9997) w/o grid	34.1	10.3% narrow 17.5% wide	1.6 5.6 16.7	0.13 0.47 1.40
GE XQ/i-2		1.25, 0.6		Q=845.2E+11.3 (R^2=1.000) with grid	33.0		1.8 5.6 18.4	0.15 0.47 1.55
GE XQ/i-2	90	1.25	244 912	N/A	28.7	7.5% narrow 13.6% wide	2.1 6.2 19.5	0.14 0.40 1.27

(nonoverlapping), 128×128 ROIs, detrending of the data, the conversion of the data to fractional values, the determination of the normalized NPS (NNPS) for each ROI by Fourier transformation, the averaging of the NNPS from the ROIs from all repeat images, computing the directional NNPS by band averaging, and rebinning the NNPS values into spatial frequency sampling intervals of 0.05 mm^{-1}.[5] The detrending step of the NPS processing aimed to remove very-low frequency trends from the image data, primarily associated with nonuniformity of the scattered radiation, a behavior that is more reflective of the geometry of the phantom than the system performance. This processing step has a negligible impact on results above 0.15 mm^{-1}.

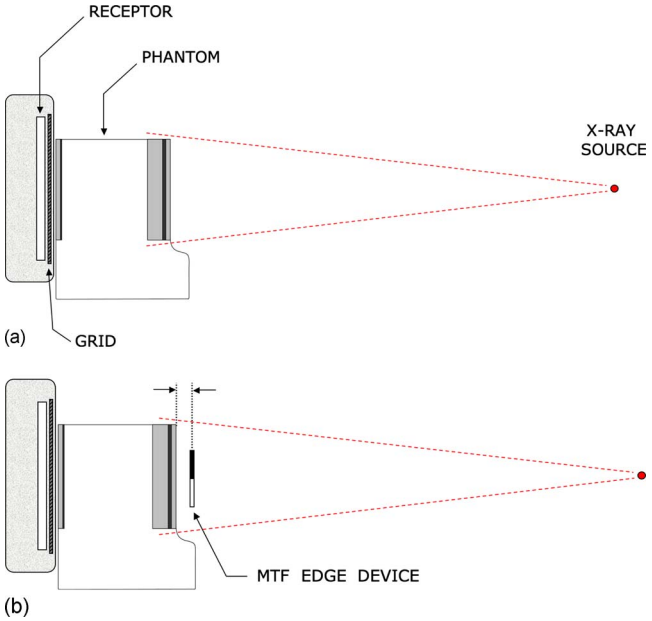

FIG. 2. Side-view schematics of acquisition geometry for the measurements of noise (a) and resolution (b) using the eDQE protocol. The MTF edge was positioned 5 cm in front of the phantom.

In general, the image acquisition targeted the assessment of the noise performance in the presence of scattered radiation and the antiscatter grid, to evaluate the system as a whole. However, to assess the relative impact of each of those elements, additional noise measurements were also made on one of the systems with the phantom, grid, or both, removed using the same mA s setting for each measurement at three different exposure levels, i.e., free-in-air exposure levels of $E_0/3.2$, E_0, and $3.2E_0$.

II.E. Resolution measurements

The resolution performance of the systems was measured with the phantom placed at the detector cover plate, as in the noise measurement setup, and was assessed with an opaque edge test device. For logistical reasons, the edge test device (TX5 W Edge Device, Scanditronix-Wellhöffer, Schwarzenbruck, Germany) was placed vertically at the center of the beam at 5 cm from the surface of the phantom (Fig. 2), facing the x-ray source, to measure the horizontal (orthogonal to

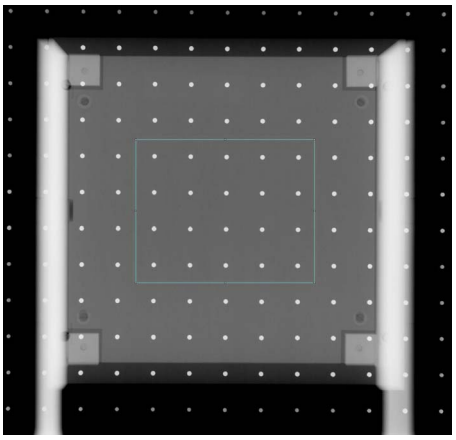

FIG. 3. An image of the beam stop device used to measure the scatter fraction within the central region depicted in the figure.

the anode-cathode axis) MTF. The positioning of the edge device enabled the assessment of the system resolution in the worst-case scenario (highest magnification) to reflect the limits of system performance. Three images were then acquired at an exposure of $3.2E_0$ at 90 kVp using the large focal spot (FS=1.25 mm) and at 120 kVp using both small (FS =0.6 mm) and large (FS=1.25 mm) focal spots.

The image data were processed to compute the MTF using established techniques.[2,24] The processing steps included the extraction of the edge region of interest, the determination of the edge angle and location in the image, the determination of the edge and line spread functions, the computation of the MTF by Fourier transformation, and averaging the MTF values into spatial frequency sampling intervals of 0.05 mm^{-1}.[5] The MTFs from three repeat images were averaged.

In general, the image acquisition targeted the assessment of the resolution performance in the presence of focal spot blur, magnification, scattered radiation, and the antiscatter grid, to evaluate the system as a whole. However, to assess the relative impact of focal spot blur, magnification, and scatter, resolution measurements were also made on one of the systems with the edge device placed at approximate surface of the phantom (at 5 cm) and at the surface of the detector cover plate without the phantom present. With the edge phantom oriented vertically, all resolution measurements were made for the horizontal direction.

II.F. Estimation of the effective detective quantum efficiency (eDQE)

The effective DQE for each system/condition was estimated using

$$\mathrm{eDQE}(f') = \frac{\mathrm{MTF}(f')^2 \cdot (1-\mathrm{SF})^2}{\mathrm{NNPS}(f') \cdot \frac{1}{m^2} \cdot \mathrm{TF} \cdot E \cdot m^2 \cdot q}, \quad (1)$$

where $\mathrm{eDQE}(f')$ is the effective DQE at magnified frequency of f' (i.e., the frequency at the entrance plane of the phantom which is given by $f'=mf$, where m is the magnification and f is the spatial frequency in the plane of the detector). $\mathrm{MTF}(f')$ is the measured MTF in the presence of phantom, scattered radiation, focal spot blur, and grid; SF is the measured scatter fraction; $\mathrm{NNPS}(f')$ is the measured normalized NPS in the presence of phantom, scattered radiation, focal spot blur, and grid; TF is the measured transmission fraction through the phantom using a narrow beam geometry; E is the measured prephantom free-in-air exposure inverse-squared corrected to that at the detector plane; and q is the ideal squared signal-to-noise-ratio per unit exposure [or $\mathrm{SNR}_{\mathrm{in}}^2$ Ref. 5] at that plane. The dimensions of the parameters are such that the units cancel, as is the case with the conventional DQE. In the denominator of Eq. (1), the $1/m^2$ factor scales the NNPS at the detector plane to that at the object plane (i.e., beam entrance surface of the phantom), while the m^2 factor applies a corresponding scaling to the exposure; the two factors effectively cancel one another. The q values, as tabulated in Table I, were estimated using an x-ray simulation routine (xSpect, Henry Ford Hospital, Detroit, Michigan) (Ref. 23) assuming an ideal counting detector with an incident primary beam attenuated by the material of the phantom.

The combined use of q, TF, and E in Eq. (1) was based on an implicit assumption that an ideal imaging system, so far as it relates to the data reported in this paper, would use a counting-type system that employs *all* the transmitted primary photons through the phantom/patient in the formation of the image but which is otherwise insensitive to scattered radiation. In this formulation, the detector-grid-cover combination is treated as the image sensor. As such, the sensor will be penalized for any primary photons absorbed by the grid or the cover but not by the attenuation of the primary photons through the phantom. Furthermore, the $(1-\mathrm{SF})^2$ factor is added to account for the low frequency drop in the MTF due to the presence of scattered radiation; our MTF processing routine includes a normalization of the MTF at zero frequency to unity which eliminates that effect, but otherwise allows the reflection of higher frequency components of the scattered radiation in the resultant MTF. Such a factor is not necessary for the NNPS as the measured results already incorporate the full effect of the scattered radiation on noise.

III. RESULTS

III.A. Phantom transmission and scatter

The phantom transmission fraction results are tabulated in Table I. The measurements are system independent but reflective of the applied beam quality; lower kVps render smaller measured phantom transmission fractions, as expected. The transmission fractions measured with the narrow beam condition were used in the eDQE calculations as described earlier. The table includes the wide-beam measurement results as a reference only. The measured phantom transmission fraction was reproducible to within 0.9% (absolute difference).

The scatter fraction results are also tabulated in Table I. They reflect higher values at 120 kVp compared to 90 kVp, as expected.[21] Repeated measurements yielded results that were reproducible to within 0.02% (absolute difference).

III.B. Noise

Figure 4 illustrates the system NNPS results (with the phantom and grid present) in the horizontal and vertical directions for the two systems at 120 and 90 kVp. The results for the systems using a small focal spot are not reported as they were very similar to those using a larger focal spot. For either system and kVp, the NNPS at the lowest exposure condition ($E_0/3.2$) is similar in the horizontal and vertical directions, except for a high frequency peak in the horizontal direction reflective of the vertical pattern of the grid lines. The appearance of the peaks associated with grid lines at 2.8/mm is a result of the grid line pattern at 7.8 lp/mm being aliased in the sampled NNPS. As the exposure increases, an additional spatially stochastic component of grid structure yields a relatively larger component of the total

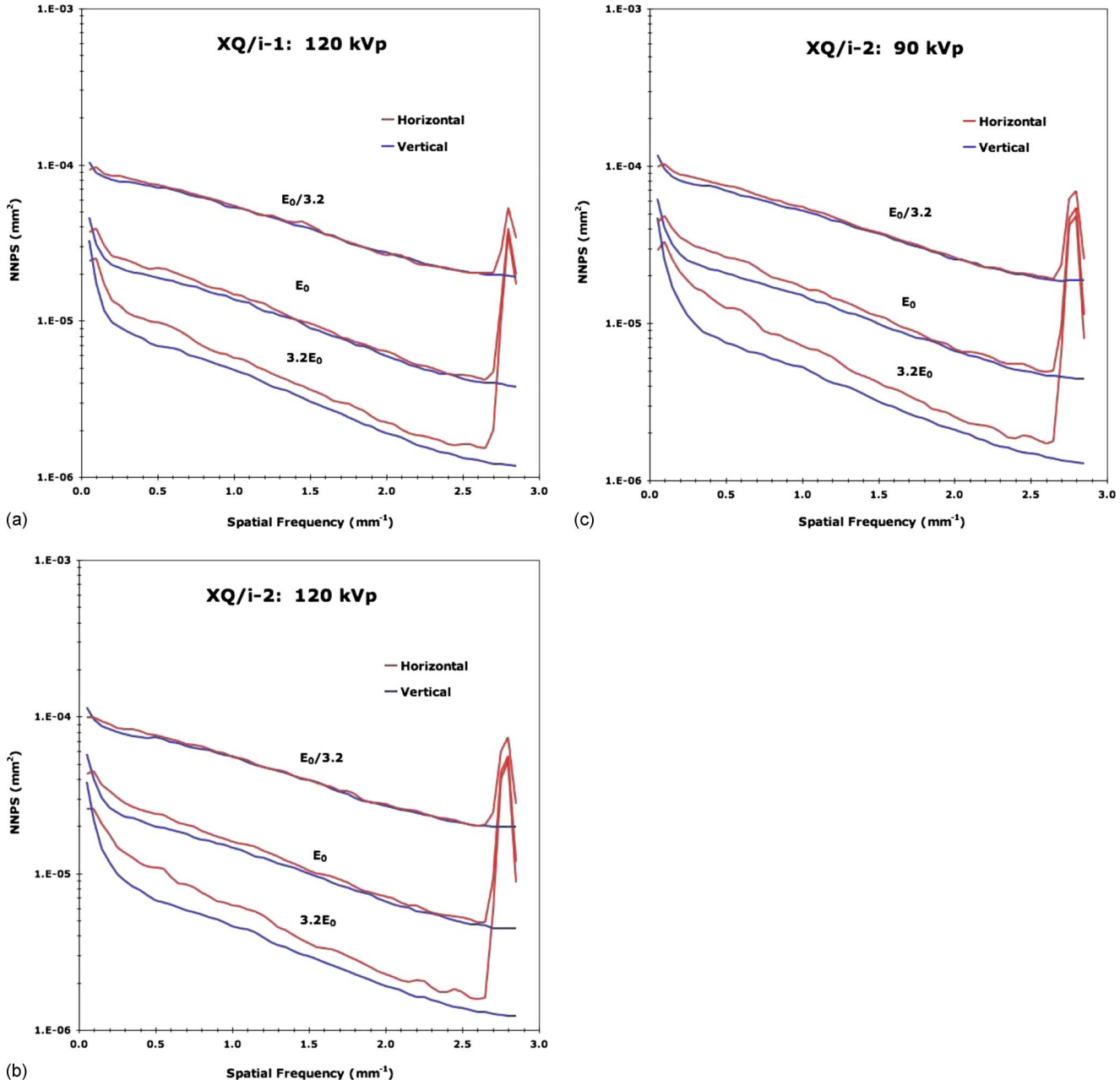

FIG. 4. The NNPS of the systems in orthogonal directions at the three evaluated exposure levels of $E_0/3.2$, E_0, and $3.2E_0$, respectively.

image noise, reflected in increased horizontal NNPS. This noise is due to nonperiodic fluctuations in the image data due to nonuniformity of grid line spacing. As most digital systems do not include the grid in the calibration process, this noise remains uncorrected within the image. The grid contribution also enhances the relative magnitude of the high frequency peaks associated with the grid lines. Repeated measurements on the same system indicated that overall the NNPS results are reproducible to within 2.1% averaged across all frequencies.

The effects of the grid (and the phantom) on the resulting NNPS are more explicitly illustrated in Fig. 5. The results indicate a higher noise magnitude with the addition of the phantom due to the beam attenuation and the added scattered radiation by the phantom. For images acquired at a constant mA s setting, the exposure to the surface of the phantom or to the sensor (when the phantom is removed) will vary as a result of these factors, yielding a change in the gross magnitude of the NPS. Higher magnitude and structure of the NNPS is also noted with the addition of the grid (due to the beam attenuation by the grid and the added grid structure). The contribution of structured noise to the NNPS is more pronounced with a higher NNPS magnitude and is associated with the presence of a characteristic peak in the horizontal NNPS, which is perpendicular to the direction of the grid lines. The grid contribution to the NNPS is also demonstrated to be exposure dependent.

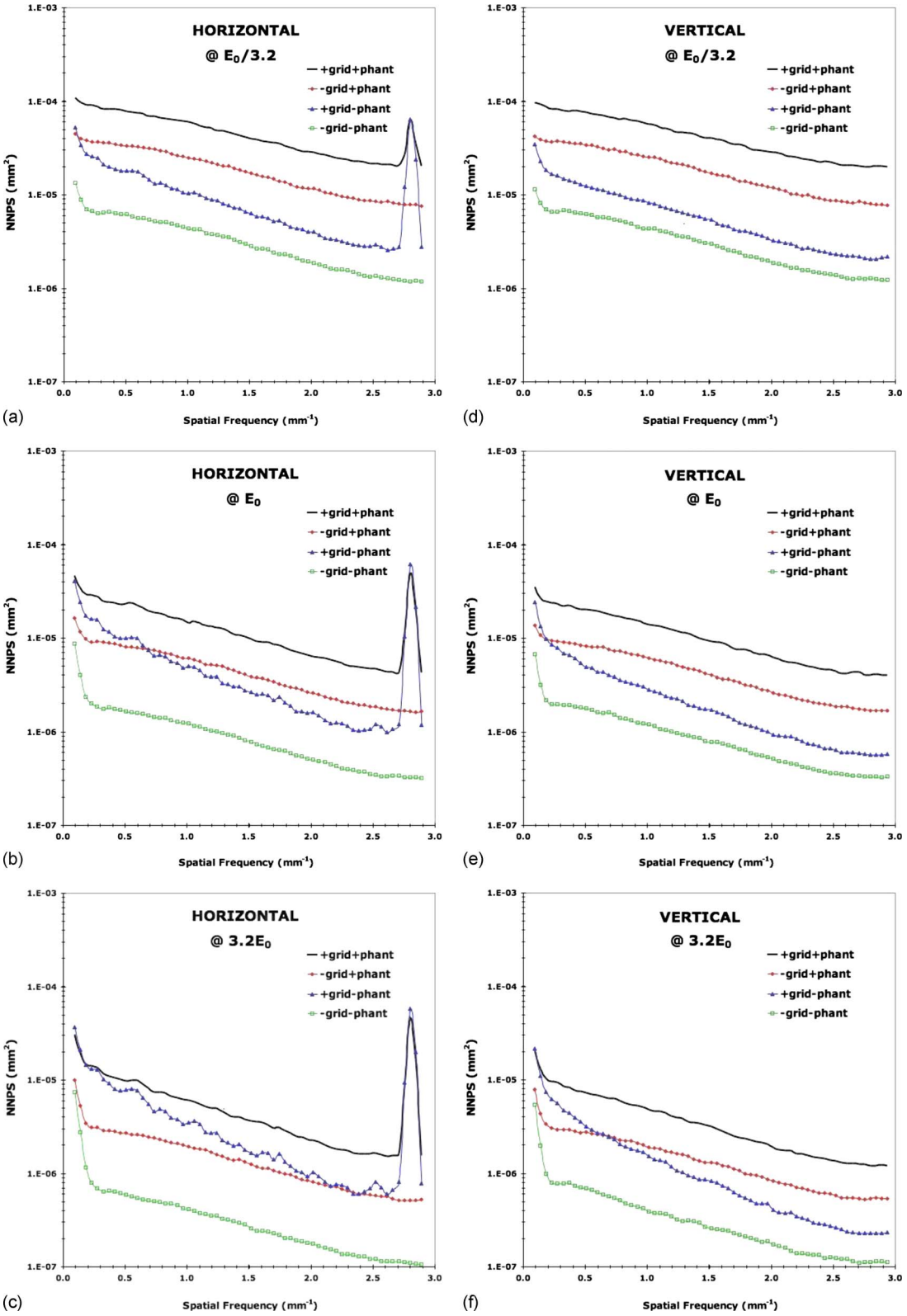

FIG. 5. The NNPS measurement with and without phantom and grid being present. All data were collected on a single system (XQ/i-1) at constant mA s values corresponding to $E_0/3.2$, E_0, and $3.2E_0$, respectively. E_0 values were as denoted in Table I whether or not attenuating materials were in place.

III.C. Resolution

Figure 6 provides a comparison of the MTF for the two different clinical systems using the eDQE standard acquisition protocol (large focal spot and 120 kVp with the grid and the phantom both present) and also demonstrates the impact of varying focal spot size and kVp for one of the systems. The results illustrate the reproducibility in the MTF measure-

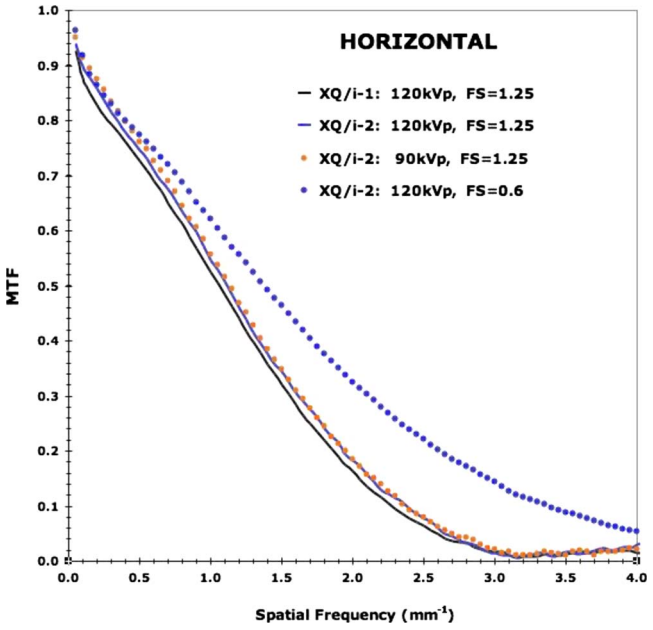

FIG. 6. The MTF results in the horizontal direction for different beam qualities and focal spot size, with phantom and grid in place. The actual system MTF would be the product of the multiplication of the reported MTFs and the associated (1−SF) factors (SF=scatter fraction reported in Table I).

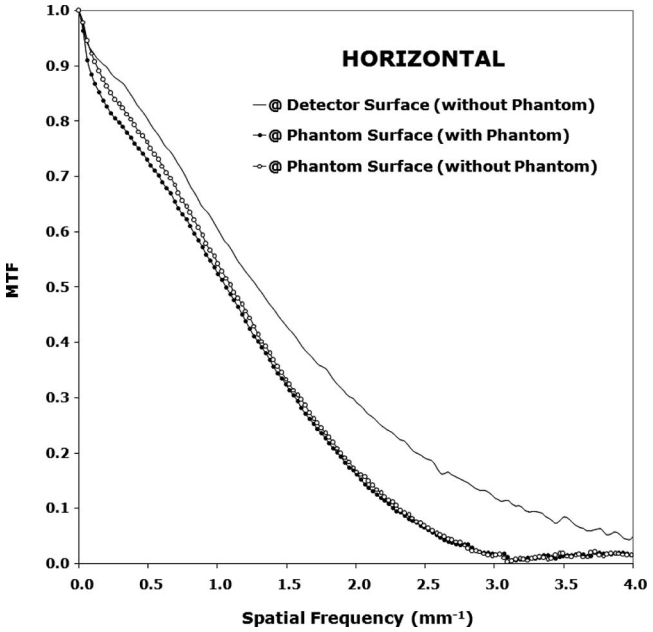

FIG. 7. The MTF results in the horizontal direction demonstrating the effects of magnification (i.e., the location of the edge test device) and the presence of the phantom for system XQ/i-1. The large focal spot (FS=1.25) was used. The actual system MTF would be the product of the multiplication of the reported MTFs and the associated (1−SF) factors (SF=scatter fraction reported in Table I).

ments from two different systems of the same make and model installed at two different institutions when using comparable large focal spots and beam qualities. The differences do not exceed 0.03 across all frequencies up to the cutoff frequency. While variations in the beam quality at 120 kVp likely have a slight impact, the majority of the difference in the MTF between these two systems is likely attributable to differences in the sizes of the focal spots since focal spot sizes are commonly different from their nominal value. Notably, on the reference system (XQ/i-1), the differences between replicated MTF measurements did not exceed 0.02 across all frequencies up to the cutoff frequency.

While the MTF appears relatively insensitive to the beam quality, the size of the focal spot has a marked effect as the system MTF is naturally reflective of both the detector performance as well as the blur caused by the focal spot magnification. The use of a small focal spot (i.e., 0.6 mm nominal size) provides a notably enhanced measured MTF, resulting from decreased focal spot blurring. As such, the MTF results reflect the actual resolution that might be obtained when using these systems to perform chest examinations on patients in the clinical setting. As these data are obtained with the edge located at the tube side of the phantom, the results are more reflective of the maximum blur for an image feature located at the posterior of the thorax (in a posteroanterior acquisition mode).

The effects of magnification and phantom (i.e., increased scatter) on the MTF are explicitly demonstrated in Fig. 7. The relative location of the edge phantom along the beam axis has a profound impact on the measured MTF, with the highest measured MTF being obtained when the edge phantom is in contact with the detector surface (magnification =1). When the edge is magnified by its placement at the surface of the phantom, the MTF is degraded. This is attributable to the increased contribution of the focal spot blur to the overall system resolution. Neither Fig. 6 nor Fig. 7 exhibit any characteristic peak associated with the grid, noted in the NNPS results shown in Figs. 4 and 5. That is due to the fact that the presampled MTF data were acquired at slight angular misalignment with respect to the exact horizontal direction; i.e., the edge was placed a few degrees from the vertical direction to obtain the presampled edge data. That process essentially removes any periodicity patterns from the resultant presampled MTF data.

Our measurement procedure for the MTF used an opaque lead edge that is sufficient to measure the detector MTF adequately but not the full extent of the scatter MTF. The results shown in Fig. 7, for example, contain a slight dip at frequencies just above the range expected for scatter (i.e., around 0.2–0.3 mm^{-1}) for the case when the scattering medium was used. This dip is around 4%. If we were able to measure the full extent of the low frequency content of the scatter, then we would have expected a dip of around 30% (i.e., equal to SF). Therefore, when we multiply the measured MTF by (1−SF), that results in a slight error in system MTF, but it should be no more than about 4%. The corresponding error in eDQE would then be expected to be about 8%.

III.D. eDQE

Combining all component results noted previously, Fig. 8 illustrates the eDQE results for the two systems, as well as

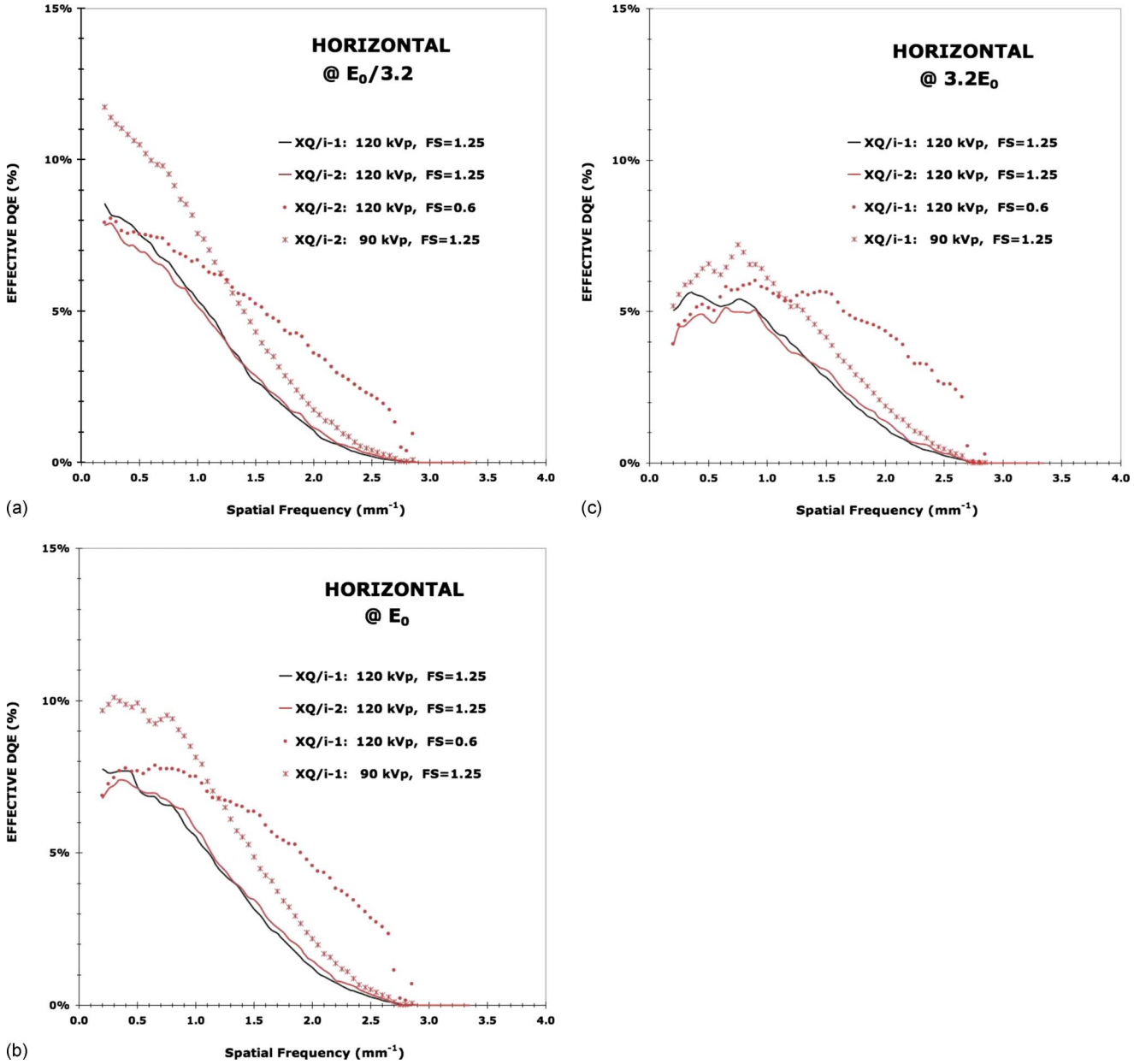

FIG. 8. The effective DQE of the reference system, XQ/i-1 at 120 kVp with a 1.25 mm focal spot in comparison with the XQ/i-2 system at 120 kVp, with 1.25 mm and 0.6 mm focal spots and at 90 kVp with a 1.25 mm focal spot. The graphs show the results in the horizontal direction at exposures corresponding to $E_0/3.2$, E_0, and $3.2E_0$, where E_0 (listed in Table I) is the free-in-air exposure level (inverse-squared corrected to the exposure at the detector) that would approximately deliver the desired target exposure to the detector ($\sim$0.4 mR) as specified by the system manufacturer.

the effects of variations in kVp and focal spot size. The figures reflect the performance in the horizontal direction at the exposure levels corresponding to $E_0/3.2$, E_0, and $3.2E_0$. The results from the two systems installed at two institutions are notably consistent. Assuming no variance associated with the measured exposure, the eDQE measurements are reproducible to within 3.0%. For each condition, the eDQE decreases with increasing exposure. This is likely due to the increased relative magnitude of structured noise associated with the grid, which was also noted in the NPS results. For a given exposure, the drops in the lower frequency range of the data are also reflective of the elevated NNPS in that zone. The improvement in the high frequency response with the use of small focal spots is also reflective of reduced focal spot blur, which was also noted in the MTF results.

The most remarkable finding of these results is the relative magnitude of the eDQE; the eDQE(0) values are in the 5%–10% range, notably short of the ideal 100% value, even for this imaging system which employs a "high-DQE" detector. These results demonstrate how significantly the scatter, magnification, focal spot blur, and grid attenuation can degrade the actual signal-to-noise performance of an imaging system.

IV. DISCUSSION

Currently, there is no universal definition of speed for digital imaging systems, leading to confusion and misapplication of the concept of analog speed[1] to digital systems. At the same time, recognizing the importance of the signal-to-noise ratio as a metric of image quality, manufacturers have strived to achieve high DQEs for these systems.[12,25–29] With the DQE performance of current detectors varying by as much as three-to-four-fold from device to device.[27,28] Without a clear definition of speed for digital systems, the higher DQEs of some digital systems, which provide the opportunity for use of lower exposure techniques, have not been adequately utilized to systematically reduce patient dose. Conversely, the use of inadequate exposure for lower DQE systems may have led to suboptimal image quality. Considering the need to obtain the best image quality at minimum patient dose, there is a clear need to define a new concept of *digital speed*, analogous to its analog counterpart for screen/film systems, that would be properly applicable to digital systems.

In digital systems, the SNR is a reasonable predictor of the image quality. As such, the speed for a digital system may be defined as that SNR that can be obtained at a given exposure to the detector or the effective dose to a reference patient (or phantom) with a typical body habitus. Such a definition would naturally be related to the DQE, the ratio of the measured SNR^2 per ideal SNR_{in}^2 that can be provided by the system given the number of incident x-ray quanta. The DQE, as defined and measured conventionally, falls short of reflecting the actual SNR efficiency of an imaging system due to its disregard for scattered radiation (an ever-present attribute of all x-ray based imaging systems), the predetector attenuation of the primary and scattered radiation by the antiscatter grid, magnification, and focal spot blur. Furthermore, the DQE is sometimes measured and reported for beam qualities and exposures not reflective of the specific application for which the system will be employed.

This study aimed to extend the concept of DQE to include the attributes of x-ray imaging that impact the actual SNR of an image. Experimentally and reproducibly measured, the new metric of eDQE reflects the actual SNR efficiency of an x-ray imaging system for a given application (chest imaging in this study), and as such can be used as a reliable definition of speed for a digital radiographic or mammographic system. A system with a higher eDQE provides a higher SNR^2 per unit incident exposure than one with a lower eDQE. With SNR^2 being linearly scalable to detection threshold based on the Rose model,[30] the eDQE would maintain a linear proportionality with intrinsic "image quality" and thus is an intuitive linear representation of speed for a digital x-ray system.

While conventional DQE is reflective of the SNR performance of a detector alone, the eDQE reflects the performance of the "system" as a whole. As such, a comparison of the DQE and the eDQE for the tested system might be particularly enlightening. Figure 9 represents the previously reported conventional DQE for the system evaluated in this study.[25] The DQE results in Fig. 9 are fivefold higher in magnitude than those of the eDQE. This suggests that the prevalent use of DQE as a comprehensive metric of image quality may need to be revisited. Furthermore, the low value of eDQE compared to the high magnitude of the DQE suggests a great opportunity for continued progress for improving the image quality of radiography and mammography systems and reducing patient dose.

This current work builds on previous work in our laboratory that included studying the effect of scattered radiation on the effective DQE of a slot scan system[31] and an evaluation of the properties of digital magnification radiography.[19] There has also been some excellent theoretical and experimental works by Kyprianou and co-workers[13–15] and Yadava *et al.*[16] in recent years evaluating the effect of scatter, focal spot blurring, and magnification on image signal-to-noise ratio; the metric derived by these investigators was called "generalized DQE" and is similar in principle to the eDQE described in this paper. Differences exist between the generalized DQE described by these other investigators and the eDQE described here: The generalized DQE works of Kyprianou and co-workers[13–15] included a specific term describing the MTF due to scatter alone. Because our eDQE formulation does not include a specific term for the scatter component of the MTF, our results and those of Kyprianou and co-workers will show differences at the very lowest spatial frequencies. While the works of Kyprianou and co-workers and Yadava *et al.* are applicable to any imaging system, its main application in literature was in the evaluation of a microangiographic system. The work presented in this current paper is the first application of an effective or generalized DQE in digital chest radiography.

Though certain generalizations can be inferred from the results of the current study, particularly the advantages of a "clinically relevant" performance metric (eDQE) over a metric measured under somewhat ideal conditions (conventional DQE), caution should be exercised before extrapolating the specific observations achieved with one single phantom geometry. Though representative of the average adult chest, the phantom employed in this study does not reflect the full range and variety of body types encountered clinically, which is especially true for chest imaging in the pediatric and bariatric ranges. It should also be noted that though the concept of eDQE can be applied to other x-ray imaging applications, care must be exercised in developing a technique and phantom combination that accurately reflects the clinical imaging geometry while accurately simulating the effects of attenuation, scatter, and magnification for the specific application of interest. The evaluation of the eDQE methodology for chest imaging applications from the pediatric range across the full range of adult chest sizes up to and including the bariatric range, extension of the technique to x-ray imaging applications beyond the chest, and independent validation using observer studies are all worthwhile objectives for future studies.

V. CONCLUSIONS

This work involved the development and assessment of a new image quality metric of the eDQE, which was designed

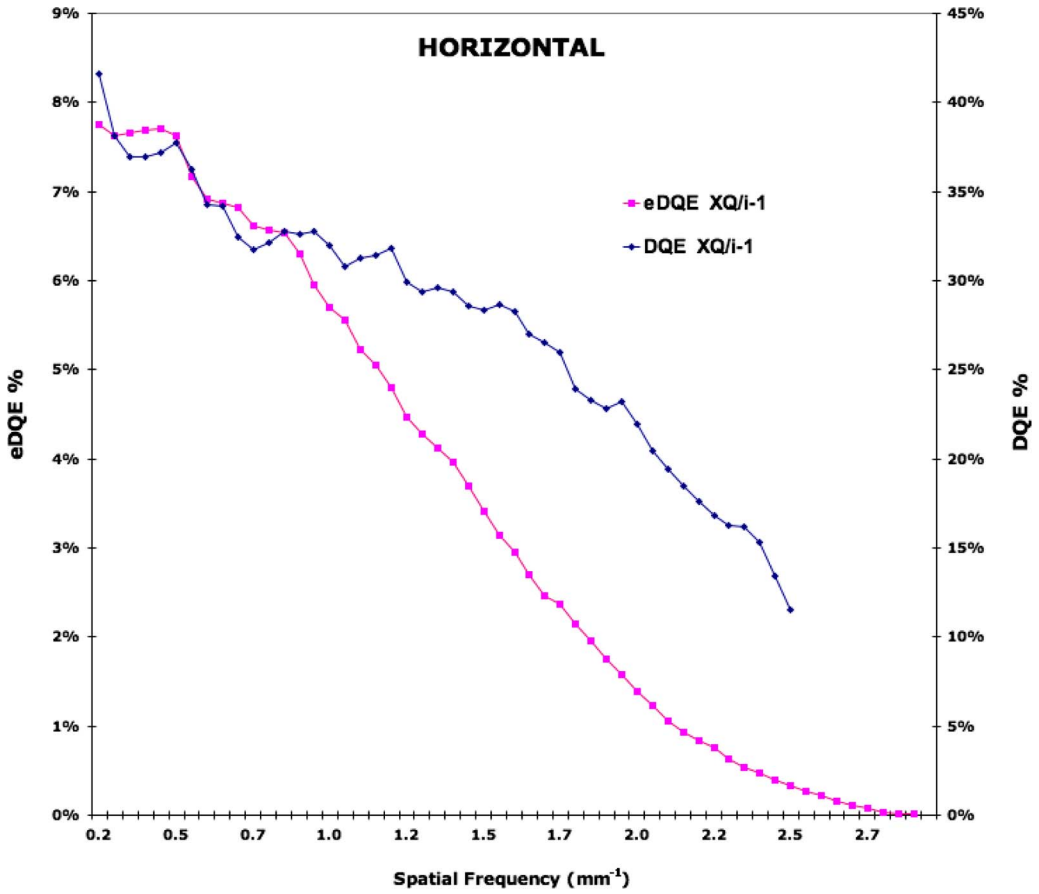

FIG. 9. The reported conventional DQE for the tested system/detector at 0.5 mR detector exposure [see Fig. 7(d), Ref. 25] at 120 kVp [RQA9 beam quality (Ref. 5)]. The DQE values are substantially higher than the corresponding eDQE values (at similar 0.5 mR detector exposure).

to reflect the actual signal-to-noise ratio performance of a digital x-ray imaging system in the presence of x-ray scattering, magnification, focal spot blur, and antiscatter grid. The findings indicated that reproducible results can be obtained using a standard measurement protocol. Its relative magnitude was found to be an order of magnitude lower than the conventional DQE, suggesting potential for additional improvements in the development of new imaging systems. The new metric of eDQE provides a more meaningful reflection of the system performance as it quantifies image quality in a more clinically relevant context. It can also serve as an application-specific definition of speed for digital x-ray imaging systems, providing an intuitive linear representation of needed exposure to achieve and maintain a target SNR.

ACKNOWLEDGMENTS

This work was supported in part by grants from the NIH (Grant Nos. R01CA109074 and R01CA80490). The authors wish to acknowledge the helpful assistance of the personnel at Duke University Hospital, Durham, NC, Guy's and St Thomas Hospital London, UK, who provided access to clinical imaging systems employed for the study.

[a]Electronic mail: samei@duke.edu

[1]ISO 9236, "Photography—sensitometry of screen-film systems for medical radiography. Part 1. Method for determination of sensitometric curve shape, speed and average gradient," (1996).
[2]E. Samei, N. T. Ranger, J. T. Dobbins III, and Y. Chen, "Intercomparison of methods for image quality characterization. I. Modulation transfer function," Med. Phys. **33**, 1454–1465 (2006).
[3]J. T. Dobbins III, E. Samei, N. T. Ranger, and Y. Chen, "Intercomparison of methods for image quality characterization. II. Noise power spectrum," Med. Phys. **33**, 1466–1475 (2006).
[4]N. T. Ranger, E. Samei, J. T. Dobbins III, and C. E. Ravin, "Assessment of detective quantum efficiency: Intercomparison of a recently introduced international standard with prior methods," Radiology **243**, 785–795 (2007).
[5]IEC 62220-1, "Medical electrical equipment—characteristics of digital x-ray imaging devices. Part 1. Determination of the detective quantum efficiency," Geneva, International Electrotechnical Commission, Geneva, Switzerland, 2003.
[6]A. D. Maidment, M. Albert, P. C. Bunch, I. A. Cunningham, J. T. Dobbins III, R. M. Gagne, R. M. Nishikawa, R. L. Van Metter, and R. F. Wagner, "Standardization of NPS measurements: Interim report of AAPM TG15, Medical Imaging 2003: Physics of Medical Imaging," Proc. SPIE **5030**, 523–532 (2003).
[7]H. Illers, E. Buhr, and C. Hoeschen, "Measurement of the detective quantum efficiency (DQE) of digital x-ray detectors according to the novel standard IEC 62220-1," Radiat. Prot. Dosim. **114**, 39–44 (2005).
[8]C. P. Lawinski, A. Mackenzie, H. Cole, P. Blake, and I. D. Honey, "Digital detectors for general radiography, a comparative technical report," Centre for Evidence-Based Purchasing Report No. 05078, 2005 (unpublished), available at http://www.pasa.nhs.uk/pasa/Doc.aspx?Path=[MN][SP]/NHSprocurement/CEP/X-ray/Report%2005078.pdf.
[9]S. Rivetti, N. Lanconelli, R. Campanini, M. Bertolini, G. Borasi, A. Nitrosi, C. Danielli, L. Angelini, and S. Maggi, "Comparison of different commercial FFDM units by means of physical characterization and contrast-detail analysis," Med. Phys. **33**, 4198–4209 (2006).

[10]P. Monnin, D. Gutierrez, S. Bulling, D. Guntern, and E. R. Verdun, "A comparison of the performance of digital mammography systems," Med. Phys. **34**, 906–914 (2007).
[11]P. E. Muntz, "Analysis of the significance of scattered radiation in reduced dose mammography, including magnification effects, scatter suppression, and focal spot and detector blurring," Med. Phys. **6**, 110–117 (1979).
[12]E. Samei, "Performance of digital radiography detectors: Factors affecting sharpness and noise," *Advances in Digital Radiography* (Radiological Society of North America (RSNA), Oak Brook, IL, 2003), pp. 49–61.
[13]I. S. Kyprianou, S. Rudin, D. R. Bednarek, and K. R. Hoffmann, "Generalizing the MTF and DQE to include x-ray scatter and focal spot unsharpness: Application to a new microangiographic system," Med. Phys. **32**, 613–626 (2005).
[14]I. S. Kyprianou, S. Rudin, D. R. Bednarek, and K. R. Hoffmann, "Study of the generalized MTF and DQE for a new microangiographic system," Proc. SPIE **5368**, 349–360 (2004).
[15]I. S. Kyprianou, A. Ganguly, S. Rudin, D. R. Bednarek, B. D. Gallas, and K. I. Myers, "Efficiency of the human observer compared to an ideal observer based on a generalized NEQ which incorporates scatter and geometric unsharpness: Evaluation with a 2AFC experiment," Proc. SPIE **5749**, 251–262 (2005).
[16]G. K. Yadava, I. S. Kyprianou, S. Rudin, D. R. Bednarek, and K. R. Hoffman, "Generalized performance evaluation of x-ray image intensifier compared with a microangiographic system," Proc. SPIE **5745**, 419–429 (2005).
[17]C. C. Shaw, X. Liu, M. Lemacks, J. X. Rong, and G. J. Whitman, "Optimization of MTF and DQE in magnification radiography—a theoretical analysis," Proc. SPIE **3977**, 467–475 (2000).
[18]S. J. Boyce and E. Samei, "Imaging properties of digital magnification radiography," Med. Phys. **33**, 984–996 (2006).
[19]B. J. Conway, P. F. Butler, J. E. Duff, T. R. Fewell, R. E. Gross, R. J. Jennings, G. H. Koustenis, J. L. McCrohan, F. G. Rueter, and C. K. Showalter, "Beam quality independent attenuation phantom for estimating patient exposure from x-ray automatic exposure controlled chest examinations," Med. Phys. **11**, 827–832 (1984).
[20]Food and Drug Administration and Conference of Radiation Control Program Directors, "Nationwide evaluation of x-ray trends: Twenty-five years of NEXT (brochure)," (2003).
[21]C. E. Floyd, J. Y. Lo, H. G. Chotas, and C. E. Ravin, "Quantitative scatter measurement in digital radiography using a photostimulable phosphor imaging system," Med. Phys. **18**, 408–413 (1991).
[22]E. Samei, Y. Lo, T. T. Yoshizumi, J. L. Jesneck, J. T. Dobbins III, C. E. Floyd, H. P. McAdams, and C. E. Ravin, "Comparative scatter and dose performance of slot-scan and full-field digital chest radiography systems," Radiology **235**, 940–949 (2005).
[23]M. J. Flynn and E. Samei, "Experimental comparison of noise and resolution for 2k and 4k storage phosphor radiography systems," Med. Phys. **26**, 1612–1623 (1999).
[24]E. Samei, M. J. Flynn, and D. A. Reimann, "A method for measuring the presampled MTF of digital radiographic systems using an edge test device," Med. Phys. **25**, 102–113 (1998).
[25]E. Samei and M. J. Flynn, "An experimental comparison of detector performance for direct and indirect digital radiography systems," Med. Phys. **30**, 608–622 (2003).
[26]C. E. Floyd, Jr., R. J. Warp, J. T. Dobbins III, H. G. Chotas, A. H. Baydush, R. Vargas-Voracek, and C. E. Ravin, "Imaging characteristics of an amorphous silicon flat-panel detector for digital chest radiography," Radiology **218**, 683–688 (2001).
[27]E. Samei and M. J. Flynn, "An experimental comparison of detector performance for computed radiography systems," Med. Phys. **29**, 447–459 (2002).
[28]E. Samei, "Image quality in two phosphor-based flat-panel digital radiographic detectors," Med. Phys. **30**, 1747–1757 (2003).
[29]M. J. Yaffe, and J. A. Rowlands, "X-ray detectors for digital radiography," Phys. Med. Biol. **42**, 1–39 (1997).
[30]A. Rose, "The sensitivity performance of the human eye on the absolute scale," J. Opt. Soc. Am. **38**, 196–208 (1998).
[31]E. Samei, R. S. Saunders, J. Y. Lo, J. T. Dobbins III, J. L. Jesneck, C. E. Floyd, and C. E. Ravin, "Fundamental imaging characteristics of a slot-scan digital chest radiographic system," Med. Phys. **31**, 2687–2698 (2004).